


PAPER

[View Article Online](#)
[View Journal](#) | [View Issue](#)Cite this: *Mater. Adv.*, 2024,
5, 8444

In situ forming PEG- ϵ -poly-L-lysine hydrogels with antimicrobial properties for fighting infection

Quanbin Dong,  Lei He, Weixue Wang, Yurong Xiong, Jine Liu, Xiaoshu Cheng* and Huihui Bao*

Most hydrogel dressings often fail to achieve the required mechanical, antibacterial, and biocompatibility properties simultaneously, which limits their clinical practical application. Therefore, it is urgent to develop a hydrogel dressing that can form *in situ* to match an irregular wound defect and have antibacterial properties. Herein, we design an *in situ* forming hydrogel composite of 4-arm-poly(ethylene glycol) succinimidyl (4-PEG-NHS) and ϵ -poly-L-lysine (PLL). This hydrogel was quickly crosslinked through reaction between the amine groups of PLL and NHS ester group of 4-PEG-NHS under physiological conditions without additional chemical crosslinking agents. Moreover, the hydrogels have inherent antibacterial properties owing to PLL, an antibacterial peptide with broad-spectrum antibacterial activity avoiding bacteria resistance. SEM results showed that the hydrogels have an appropriately interconnected porosity, which facilitates the exchange of nutrients and oxygen with tissues. The swelling results indicated their excellent water absorption and retention capacity, which can not only absorb a large amount of wound exudate but also maintain the wet environment of the wound to accelerate wound repair. The PEG-PLL hydrogels have been found to have excellent antibacterial activity against Gram-positive (*S. aureus*) and Gram-negative (*E. aureus*) bacteria *in vitro*. In an SD rat full-thickness skin defect infection model, the PEG-PLL hydrogels showed a significant antibacterial effect and higher wound closure ratios. Furthermore, the cytotoxicity and hemolytic results indicated that PEG-PLL hydrogels have excellent biocompatibility. In summary, PEG-PLL hydrogels are an ideal wound dressing in clinical work for irregular infected wound repair.

Received 18th March 2024,
Accepted 30th May 2024

DOI: 10.1039/d4ma00287c

rsc.li/materials-advances

1. Introduction

As the body's first line of defense, skin plays an important role in immunity as a physical barrier. When the skin is damaged, especially in patients with diabetes and hypo-immunity, external bacteria can easily colonize and multiply in the wound, thus causing pain, suppuration, and other symptoms of infection, greatly delaying the healing of the wound.^{1,2} If the infection is not well controlled, it is probable that it will cause deep tissue or even systemic infection, significantly raising medical costs. In the United States, approximately 6.5 million patients suffer from chronic wounds each year, and the cost of wound medical care is approximately \$25 billion.¹ In Europe, the cost of wound treatment is estimated to be €4–6 billion per year.³ Therefore, suitable wound dressings are of great significance for wound coverage, antibacterial properties and wound repair.^{4,5}

A wet environment is more beneficial to wound healing, which has been proven in many studies.^{6,7} Hydrogels are widely

used as wound dressings due to their similarity to the extracellular matrix (ECM) and their ability to maintain a wet environment.^{8–10} Recently, a hybrid hydrogel based on carbonylmethyl chitosan and sodium alginate was designed to accelerate wound repair.¹¹ Hon *et al.*¹² developed polysaccharide-peptide cryogels as a wound dressing for wound healing. However, this type of hydrogel was preformed, so it could not fit tightly to irregular wounds during use and could easily fall off. Compared with preformed hydrogels, *in situ* forming hydrogels have significant advantages. They not only can match irregular skin defects but also can be physically isolated to protect the skin defect from infection.^{13,14} Hydrogel dressings can provide a moist environment to promote tissue repair, but also increase the chance of wound infection, so hydrogel dressings need to have antibacterial properties.^{15,16} Many antibacterial hydrogels developed for wound repair recently are based on silver nanoparticles or antibiotics. For instance, bacterial cellulose hydrogels containing silver nanoparticles were developed and exhibited antimicrobial activity against bacteria. Makvandi P. *et al.*¹⁷ prepared hyaluronic acid hydrogels loaded with nano-silver as a wound dressing. Jayanta Haldar *et al.*¹⁸ designed aminoglycoside hydrogels cross-linked

Department of Cardiology, The Second Affiliated Hospital of Nanchang University,
No. 1 Minde Road, Nanchang 330006, Jiangxi, P. R. China.
E-mail: xiaoshumenfan@126.com, huihui_bao77@126.com



by oxidized dextran and aminoglycoside, and they were found to have excellent antibacterial activity. However, nano-silver may accumulate in the body and endanger human health, and the widespread use of antibiotics may lead to antibiotic resistance.^{19,20} Therefore, an ideal hydrogel dressing should be *in situ* forming, have excellent biocompatibility and antibacterial properties, but not cause antibiotic resistance.

4-Arm-poly ethylene glycol (4-arm-PEG) is an important material for developing hydrogels for application in tissue repair due to its high water solubility, non-immunogenicity, non-toxicity and degradability.^{21–23} Furthermore, the PEG hydrogel has unique inherent protein adsorption and cell adhesion capabilities, making it a preferred choice for building biomaterials. The 4-Arm-PEG hydrogel has a nearly ideal network structure and excellent performance and has great application potential in biomedical materials.^{24,25}

ϵ -poly-L-lysine (PLL) is one of the antimicrobial peptides having broad-spectrum antibacterial properties.²⁶ Moreover, it is biodegradable, edible, has high water-solubility and heat-stability and is non-toxic towards humans. All these advantages offer PLL a wide range of applications in the antibacterial field. Recently, PLL has been modified with meth-acrylamide moieties, and then crosslinked with PEG diacrylate to form antibacterial hydrogels.^{27,28} This hydrogel has low hemolysis, excellent cytocompatibility and antibacterial activity *in vitro*. The antibacterial wound dressing was prepared by chemical modification of PLL into a nanofiber matrix. Moreover, PLL does not easily become drug-resistant compared with antibiotics, and the reason is that PLL mainly destroys the integrity of microbial membranes.^{29,30}

Therefore, we developed a PEG–PLL hydrogel composite of 4-arm-poly(ethylene glycol) succinimidyl (4-arm-PEG-NHS) and PLL which can form *in situ* through the reaction between the NHS ester groups in 4-arm-PEG-NHS and amino groups in PLL under physiological conditions without an additional cross-linking agent (Fig. 1). Moreover, the NHS ester group can react with the amino groups present on the tissue surface resulting in tissue adhesion. The swelling results indicated that

hydrogels have excellent water absorption and water retention, which can not only absorb a large amount of wound exudate, but also maintain the wound wet environment to accelerate wound repair. Furthermore, the cytotoxicity and hemolytic results indicate that PEG–PLL hydrogels have excellent biocompatibility. The PEG–PLL hydrogels showed a significant antibacterial effect, higher wound closure ratios and collagen deposition in a rat full-thickness skin defect infection model. In brief, PEG–PLL hydrogels are an ideal wound dressing in clinical work for irregular wound repair, especially for infected wounds.

2. Materials and methods

2.1. Materials

4-Arm-poly(ethylene glycol) succinimidyl (4-PEG-NHS, $M_w = 20$ kDa) was purchased from Xiamen Sinopeg Biotech Co., Ltd. ϵ -poly-L-lysine (PLL, $M_w = 3.5$ kDa) was purchased from Zhengzhou bainafo Bioengineering Co., Ltd. The NIH 3T3 cells were purchased from the Chinese Academy of Sciences Cell Bank. *Escherichia coli* (*E. coli*, #25922) and *Staphylococcus aureus* (*S. aureus*, #25923) were obtained from American Type Culture Collection. The Cell Counting Kit-8 (CCK-8) was purchased from Shanghai Beyotime Biotech Co., Ltd. The live/dead cell staining kit was purchased from Invitrogen (Carlsbad, USA). Dulbecco's modified Eagle's medium (DMEM) and fetal bovine serum (FBS) were purchased from Gibco. Other reagents were purchased from Sigma-Aldrich. Unless otherwise specified, all reagents and chemicals are commercially available and of analytical grade before use and do not require further purification.

2.2. Preparation of PEG–PLL hydrogels

To obtain two-component injectable hydrogels, 4-PEG-NHS and PLL were dissolved in PBS (pH = 7.4). In brief, 300 mg 4-PEG-NHS powder was dissolved in 1 mL PBS (30% w/v). 20 mg, 60 mg, 100 mg, and 200 mg PLL powder were dissolved in 1 mL

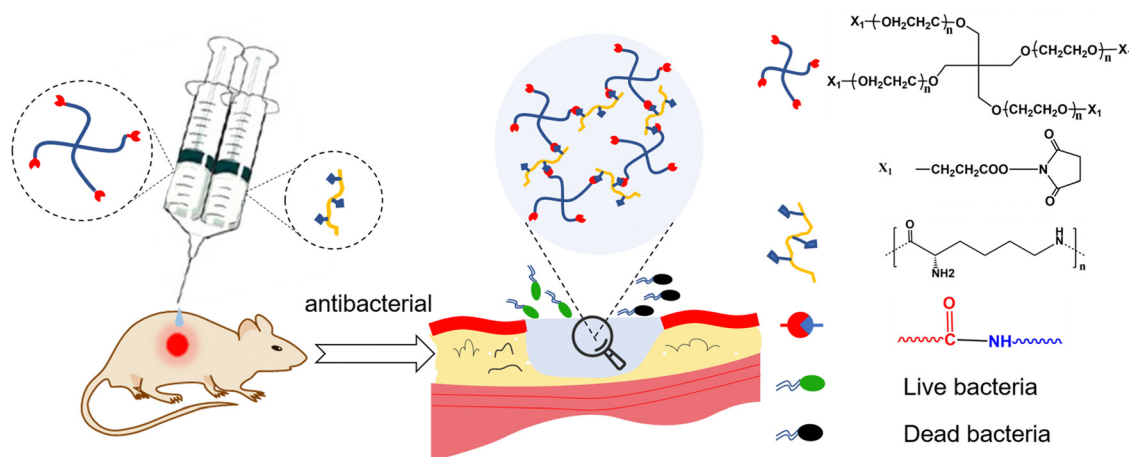


Fig. 1 Schematic illustration of *in situ* forming PEG–PLL hydrogels with antibacterial properties for wound repair.



PBS respectively (2, 6, 10, and 20% w/v) to obtain different concentrations of PLL solution and the PLL solution (pH = 7.4) was adjusted to pH = 8 with NaOH solution. Then, an equal volume of precursor solution of 4-PEG-NHS and different concentrations of PLL solution were simultaneously injected to form the PEG-PLL hydrogels. The PEG-PLL hydrogels with different PLL contents (1, 3, 5, and 10 wt%) were named PEG-PLL (1), PEG-PLL (3), PEG-PLL (5) and PEG-PLL (10), respectively.

2.3. Rheological test

The viscoelastic properties of the PEG-PLL hydrogels were performed at 37 °C on a HAAKE MARS III advanced rotary rheometer. Briefly, 100 µL of precursor solution 4-PEG-NHS and 100 µL PLL were simultaneously injected to form hydrogels in a cylindrical mold with a diameter of 10 mm and a height of 3 mm. Then the hydrogels were placed on a plate of a rotary rheometer. The modulus test was performed at the controlled strain (CD) mode, with a 0.1% strain and a frequency of 1 Hz. A frequency-dependent rheology measurement for the hydrogels was performed at a 1% strain amplitude (γ) with the frequency change from 0.1 Hz to 2.5 Hz. The storage modulus (G') and loss modulus (G'') values were recorded.

2.4. Effect of pH on the gelation time and rheological properties of PEG-PLL hydrogels

pH is an important factor that can affect the crosslinking speed of PEG-PLL hydrogels by affecting the amino activity on PLL. Therefore, we tested the influence of pH on the gelation time and rheological properties of PEG-PLL hydrogels. The PLL solution (10 wt%) was adjusted to different pH values and an equal volume of 4-arm-PEG-NHS (pH = 7.4) solution was simultaneously injected to form the PEG-PLL hydrogels. The gelation time and rheological properties were tested. The gelation time is the time from mixing 4-PEG-NHS and PLL to reaching a nonflowing state. After hydrogel gelation, the HAAKE MARS III advanced rotary rheometer was used to test the rheological properties.

2.5. Swelling test

100 µL 4-arm-PEG-NHS solution and 100 µL PLL solution were simultaneously injected into a cylindrical mold with a diameter of 10 mm and a height of 3 mm to form hydrogels. The preformed hydrogel was transferred into the 24-well plate and immersed in 2 mL of PBS at 37 °C. Then the hydrogel was carefully dried with absorbent paper and weighed at different time points (2, 4, 8, 12, and 24 h). When the quality of the hydrogel no longer increases, the swelling balance is reached. Then, the swollen hydrogel is stored at −21 °C overnight, and freeze-dried for 72 h. The swelling ratio at different time points is calculated as follows: $W_t = (m_t - m_0)/m_0 \times 100\%$, m_0 is the initial gel mass, and m_t is the gel mass at the corresponding time point. The water absorption of the hydrogel is calculated as follows: $\text{water absorption}\% = (m_s - m_d)/m_s$, m_s is the gel mass at the swelling balance and m_d is the dry weight of the hydrogel.

2.6. Scanning electron microscopy (SEM)

100 µL of precursor solution 4-PEG-NHS and 100 µL PLL were simultaneously injected to form hydrogels in a cylindrical mold with a diameter of 10 mm and a height of 3 mm. Then PEG-PLL hydrogel sample was first stored at −21 °C overnight, and freeze-dried for 72 h. Next, the lyophilized hydrogel was frozen under liquid nitrogen, and cut to obtain the sample surface. The surface was sprayed with gold and photographed with a scanning electron microscope (SEM, S-4800, HITACHI).

2.7. Fourier transform infrared spectroscopy

PEG-PLL hydrogels were freeze-dried and ground into powder, and 4-arm-PEG-NHS powder was used as the control sample. The results for the two samples were obtained through Fourier transform infrared spectroscopy using a TENSOR-27 spectrometer (Bruker, German).

2.8. Cytotoxicity studies

We use high-pressure sterilization of PEG and PLL solutions before *in vitro* testing. The PEG-PLL hydrogel cytotoxicity test was evaluated using the Cell Counting Kit-8 (CCK-8) method. In brief, the NIH 3T3 cells were collected from a 10 cm cell plate and the cell concentration was diluted to $5 \times 10^4 \text{ mL}^{-1}$ by adding 100 µL of the cell dilution suspension to a 96-well plate to culture the cells for 1 d (37 °C, 5% CO₂). 0.4 mL of PEG-PLL hydrogel was immersed in 4 mL of serum-free DMEM culture solution for 1 d (37 °C). Then, the extracted DMEM solution is added with 10% FBS to culture 3T3 cells (37 °C, 5% CO₂). After 24 hours of culture, the cell culture solution was removed, and 100 µL of DMEM containing 10 µL CCK-8 were added to each well. After cell incubation for 2 h, the OD value at 450 nm was measured using a microplate reader. The formula for calculating the cell survival rate is as follows: $\text{cell viability} (\%) = (\text{average absorbance of the hydrogel group} / \text{average absorbance of the control group}) \times 100\%$. The final experimental results were obtained from three parallel experiments.

A live-dead assay was also used to evaluate the biocompatibility of the PEG-PLL hydrogel. The NIH 3T3 cells were seeded in a 24-well plate (25 000 cells per plate), and then co-cultured with the hydrogel extract for 1 d (37 °C, 5% CO₂). Finally, the cells were stained with a live-dead assay kit (Invitrogen, USA), and observed and photographed using a confocal microscope (Leica, inverted fluorescence microscope).

2.9. Hemolysis assay

A rabbit blood sample was collected with an EDTA anticoagulation tube, and kept at 4 °C until use. 5 mL of rabbit blood sample were centrifuged at 3000 rpm for 5 min to separate the red blood cells (RBC). Then the RBCs were washed 3 times with PBS buffer to obtain a 5% (v/v) red blood cell solution in PBS buffer. 200 µL of PEG-PLL hydrogel containing different concentrations of PLL were immersed in 1 mL of RBC solution and incubated at 37 °C for 1 h with a shaking rate of 150 rpm, then the samples were centrifuged at 3000 rpm for 5 min to obtain the supernate. Finally, 100 µL supernate was transferred into a



96-well plate, and the absorbance value at 450 nm was measured using a microplate reader. We used 0.1% Triton x-100 as a positive control and PBS buffer as a negative control. The formula for calculating the hemolysis rate is as follows: hemolysis (%) = $(A_p - A_b)/(A_t - A_b) \times 100\%$, where A_p is the absorbance value of the hydrogel group, A_b is the absorbance value of the PBS buffer group, and A_t is the absorbance value of the Triton x-100 group. The final experimental results are obtained from three parallel experiments.

2.10. Antimicrobial ability determined *in vitro*

The inhibition zones of bacteria were used to evaluate the antibacterial ability of PEG-PLL hydrogels. Gram-positive (*S. aureus*) and Gram-negative (*E. coli*) bacteria were respectively selected to evaluate the antibacterial ability of the PEG-PLL hydrogel *in vitro*. Briefly, *E. coli* and *S. aureus* were respectively cultured in LB and Tryptic Soy Broth medium at 37 °C for 12 hours. Then, 100 μ L (10^7 CFU per mL) of the bacterial solution was evenly coated on the surface of the Tryptose Soya Agar. The surface of the culture medium was drilled with a 6 mm Oxford cup, 200 μ L of the PEG-PLL hydrogels with different PLL content was injected, and PBS buffer was used as a negative control. After 1 d incubation at 37 °C, the inhibition zones of the bacteria were imaged and measured using Wanshen software. The final experimental results are obtained from three parallel experiments.

2.11. Antimicrobial and wound repair assessment *in vivo*

All rats were purchased from Shanghai Jiagan Biotechnological Company. Procedures involving animals and their care were performed following NIH guidelines, and approved by the Ethics Committee of the second affiliate hospital of Nanchang University. A male SD rat (8 weeks, 250–300 g) full-thickness skin defect infection model was used to evaluate the antibacterial and wound repair effect of the PEG-PLL hydrogels. The rats were anesthetized with chloral hydrate (10 wt%) and the dorsal hair was removed. Then, the skin drill was used to make three round full-thickness defects (10 mm in diameter) on the dorsal skin under sterile conditions, for a total of six rats. 500 μ L saline was used for the control group. 100 μ L *S. aureus* (10^9 CFU per mL) were added to the bacterial and hydrogel groups for 2 hours. Then, we injected 4-arm-PEG-NHS and PLL into the local wound site to form a hydrogel *in situ* using a two-component syringe. The wound healing was observed and photographed at regular intervals (4, 7, and 11 d) after the operation, and the diameter of the wound was measured with a ruler until it healed completely. The formula for calculating the wound healing rate is: Wound closure ratio (%) = $(W_2 - W_1)/W_2 \times 100\%$. W_2 is the original wound area, and W_1 is the wound area at the observation time.

2.12. Histopathological examination

To evaluate bacterial infection and wound repair in each group, tissues around the wound were collected on day 7 and day 11, washed sequentially with 0.9% saline, fixed in 4% paraformaldehyde for 24 hours, dehydrated with gradient ethanol, made

transparent with xylene, and finally made into 5 μ m paraffin sections. Finally, the paraffin sections were stained with H&E and Masson and then observed through optical microscopy (Leica).

2.13. Statistical analysis

All data were expressed as mean \pm standard deviation (SD). All statistical analysis was performed using Graph pad Prism 8.

3. Results and discussion

3.1. Preparation and characterization of the PEG-PLL hydrogels

The PEG-PLL hydrogels were crosslinked by the reaction between the NHS ester groups of 4-arm-PEG-NHS and amino groups of PLL under physiological conditions which is widely used to construct hydrogels *in situ* (Fig. 1). Moreover, the NHS ester group can react with the amino group on the surface of tissue. The advantages of mild reaction conditions, fast gelation speed, and good controllability of the hydrogenation system constructed based on this mechanism of gelation have attracted widespread attention in the tissue engineering field.

The rheological properties of the PEG-PLL hydrogels were tested at 37 °C using a HAAKE MARS III advanced rotary rheometer. As shown in Fig. 2A, with the increase of PLL content, the storage modulus (G') increased from 500 to 2500 Pa. This indicates that the NHS ester group of 4-PEG-NHS can quickly react with the amino group of the PLL, and it also shows that different viscoelastic properties can be obtained by adjusting the concentration of PLL. However, the results show that the storage modulus (G') does not increase after the PLL content reaches 5 wt%. A possible reason is that the over-crosslinked state will hinder the free movement of the PEG molecules, and the mechanical properties of the hydrogel are not increasing. A frequency-dependent rheology measurement for the PEG-PLL hydrogels was obtained from 0.1 Hz to 2.5 Hz at 1% strain amplitude (γ). As shown in Fig. 2B, as the PLL concentration increases, the storage modulus (G') values increase, indicating that the gel state of the hydrogel is maintained and the hydrogel has good mechanical stability.

After local tissue damage, reactive exudation will appear around the wound, especially in patients with diabetes who have a large amount of exudate. Hydrogels can not only absorb a large amount of wound exudate, but also maintain the wet environment of the wound to accelerate wound repair, making them ideal for wound dressings. Therefore, we tested the swelling ratio and water absorption ratio of PEG-PLL hydrogels with different PLL contents. As shown in Fig. 2C, the swelling equilibrium was basically reached at about 12 hours. The swelling ratio even reached 250% with the increase of the PLL content.

We also investigated the water absorption capacity of PEG-PLL hydrogels with different PLL contents. After lyophilization, the PEG-PLL hydrogels could absorb 14 to 23 times the water itself to reach swelling balance, and the water absorption ratio



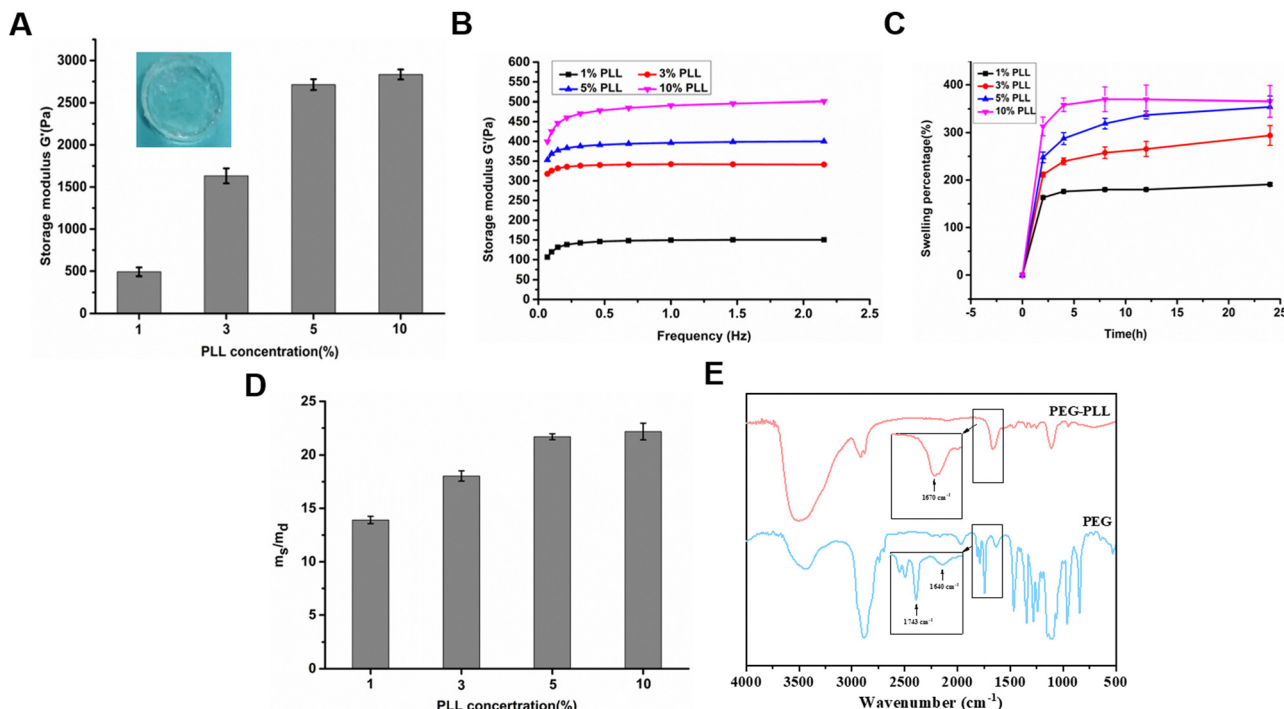


Fig. 2 Characterization of the PEG-PLL hydrogel. (A) The final storage modulus (G') of the PEG-PLL hydrogels with a strain amplitude of 0.1% and a frequency of 1 Hz at 37 °C. (B) Rheology analysis of the PEG-PLL hydrogels using frequency-dependent rheological measurement with a frequency sweep from 0.1 to 2.5 Hz and a fixed strain amplitude of 1% at 37 °C. (C) The swelling curve of PEG-PLL hydrogels at different time points (2, 4, 8, 12, and 24 h). (D) The water absorption ratio of the PEG-PLL hydrogels. (E) FTIR spectra of 4-arm-PEG-NHS and PEG-PLL.

increased with the increase of the content of PLL (Fig. 2D). A possible reason is that the cross-linking density of the hydrogel network decreases as the PLL content increases. We also found that there is little difference in swelling ratio and water absorption ratio between PEG-PLL (5) and PEG-PLL (10) hydrogels. The reason is that an over-crosslinked state will hinder the free movement of the PEG molecules, and the mechanical properties of the hydrogel are not increasing. The reason for this phenomenon is that excessive PLL can cause poor stretching of 4-PEG-NHS molecules. The results show that the PEG-PLL hydrogels have excellent water absorption and water retention capabilities which make the hydrogel quickly absorb exudate fluid around the wound and provide a wet environment for accelerated wound repair.

To testify to the reaction between the NHS ester groups in 4-arm-PEG-NHS and amino groups in PLL, the chemical structures of PEG-PLL were characterized by FTIR analysis. As shown in Fig. 2E, the characteristic peak at 1743 cm^{-1} representing C=O stretching of N-hydroxysuccinimide of 4-arm-PEG-NHS disappears after the formation of the PEG-PLL hydrogel, while a new peak was observed at 1670 cm^{-1} that can be assigned to the N-H bending vibration of amide. These results are consistent with our hypothesis that PEG-PLL hydrogels were crosslinked by amide bonds.

According to the above results, we can determine that the PEG-PLL hydrogels can be simply obtained by mixing 4-PEG-NHS and PLL solution. The conditions for amine groups and NHS ester groups to react and form amide groups are mild and

no additional cross-linking agent is needed. The PEG-PLL hydrogels have adjustable mechanical properties and excellent water absorption and retention capacity. In a word, PEG-PLL hydrogels are very suitable and convenient for clinical use as dressings.

3.2. Effect of pH on PEG-PLL hydrogels in terms of gelation time and rheological properties

The PEG-PLL hydrogel is a bi-component injectable hydrogel that can be used in irregular tissue defects. When the two components are mixed, they can gradually crosslink to form a hydrogel. To facilitate clinical operation and application, suitable gelation time is crucial. If it takes too long to gel, it will delay the operation time. If the gelation time is too short, there will be no time to operate before gelation. A gelation time of 5–10 s is more suitable for clinical mixing and injecting. PLL is composed of 25–35 lysine monomers and is a polyvalent cation that can bind with anionic substances. A change in pH results in a protonation process. Under acidic conditions, the side chain amino groups obtain hydrogen ions to form positively charged NH_3^+ , which has strong electrophilicity. Under alkaline conditions, the amino group is a typical nucleophilic reagent. Therein, different pH values can influence the gelation time and rheological properties by influencing the activity of amino groups. In this experiment, PEG-PLL (5) was used to investigate the effects of different pH values on the gelation time and rheological properties of PEG-PLL hydrogels.



Table 1 The effect of pH on gelation time and rheological properties

Number	pH	Gelation time (s)	G' (Pa)	G'' (Pa)
1	6.15	82	921.6 ± 17.12	2.16 ± 2.41
2	7.0	11	1216.1 ± 43.49	65.9 ± 3.72
3	7.4	9	1927.6 ± 75.13	97.1 ± 2.55
4	8.0	6	2961.6 ± 86.92	170.6 ± 8.32
5	8.6	3	2231.1 ± 81.18	146.9 ± 12.70

As shown in Table 1, the pH had a great influence on the gelation time and viscoelasticity of PEG-PLL hydrogels. The gelation time decreased from 82 s at pH = 6.15 to 3 s at pH = 8.6, and the storage modulus (G') increased from 921.6 Pa to 2961.6 Pa, but the storage modulus (G') decreased when the pH reached 8.6. The results show that pH has a significant effect on gelation time and viscoelasticity. The higher activity of $-NH_2$ leads to a shorter gelation time and higher storage modulus (G'). Therefore, PEG-PLL has a suitable gelation time and viscoelastic properties at pH 7.4, and the PEG-PLL hydrogels used in subsequent experiments were all configured at pH = 7.4. Moreover, the appropriate pH around the skin is 7.2–7.4.

3.3. Morphology of hydrogels

Porosity is an important parameter for the diffusion of oxygen and nutrients between a hydrogel and the surrounding tissue. We used SEM to explore the microstructure of the PEG-PLL hydrogels. Cross-sections of the PEG-PLL hydrogels are shown in Fig. 3. It can be found that all hydrogels show a highly interconnected and porous three-dimensional network structure. Interconnected pores enhance the diffusion of oxygen and nutrients from the surrounding area to the hydrogel. The pore sizes of PEG-PLL hydrogels range from 5 μ m to 50 μ m corresponding to PLL concentrations from 1% to 10%. But there is no significant difference in the pore size between PEG-PLL (5) and PEG-PLL (10). To promote wound repair, the pore size of the

hydrogel must be greater than 20 μ m which is beneficial to vascular regeneration. In conclusion, the PEG-PLL (5%) hydrogel exhibits excellent viscoelasticity, water absorption and suitable pore size. Therefore, the PEG-PLL (5%) hydrogels were used in subsequent *in vivo* experiments.

3.4. Biocompatibility of PEG-PLL hydrogels

Hydrogels should have excellent biocompatibility when used as wound dressings. Cytotoxicity is considered to be one of the most important factors for evaluating the biocompatibility of hydrogels. NIH 3T3 cells were seeded in a 96-well plate (5000 cell per plate) and cultured for 24 hours (37 $^{\circ}$ C, 5% CO_2), and then co-cultured with different hydrogel group extracts for 24 hours. During the culture period, 3T3 showed high cell viability in the PEG-PLL (1), PEG-PLL (3) and PEG-PLL (5) hydrogel groups (Fig. 4A); 92.72%, 96.73%, and 82.76%, respectively. However, we can see that the cell viability in the PEG-PLL (10) group is lower than 80%. A possible reason is that excessive positive charge accumulated on PLL can affect the negative charge on the cell membrane and decrease cell survival.

We evaluated the hemocompatibility of PEG-PLL hydrogels by mixing the RBCs and hydrogels. PBS and Triton-100 were selected as the negative and positive controls respectively. As shown in Fig. 4B, all the hydrogels show negative hemolysis and the hemolytic ratio is slightly increased with the increased PLL content. The hemolytic ratio of PEG-PLL (1%) is only 0.347%, while the hemolytic rate of PEG-PLL (10) is up to 4.11%. These results show that PEG-PLL (5) hydrogels cause less damage to red blood cells and are safe to use as wound dressings.

We then performed live/dead cell viability assays to study the effect of PEG-PLL (5) hydrogels on cell viability. The PEG-PLL (5) hydrogel extract was cultured with 3T3 cells. Almost only green fluorescent 3T3 cells were observed, and there was no

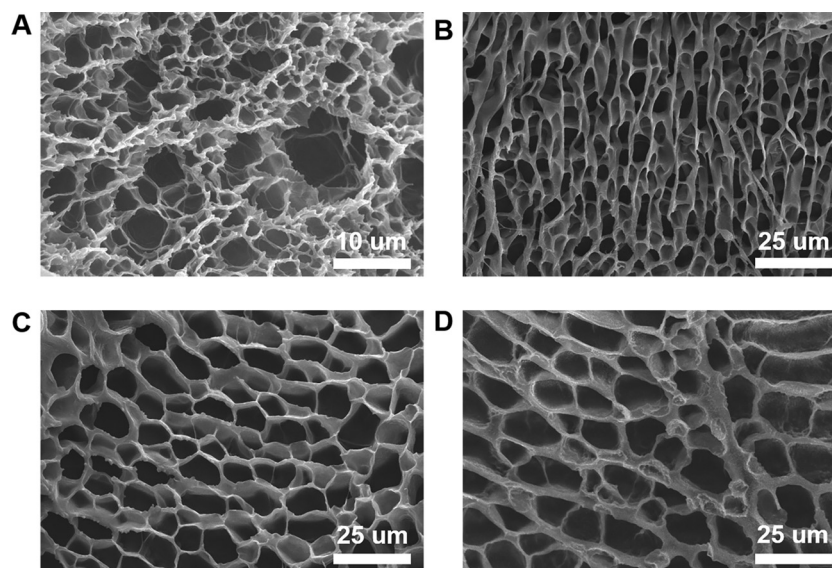


Fig. 3 SEM images of (A) PEG-PLL (1) hydrogels, (B) PEG-PLL (3) hydrogels, (C) PEG-PLL (5) hydrogels, and (D) PEG-PLL (10) hydrogels.



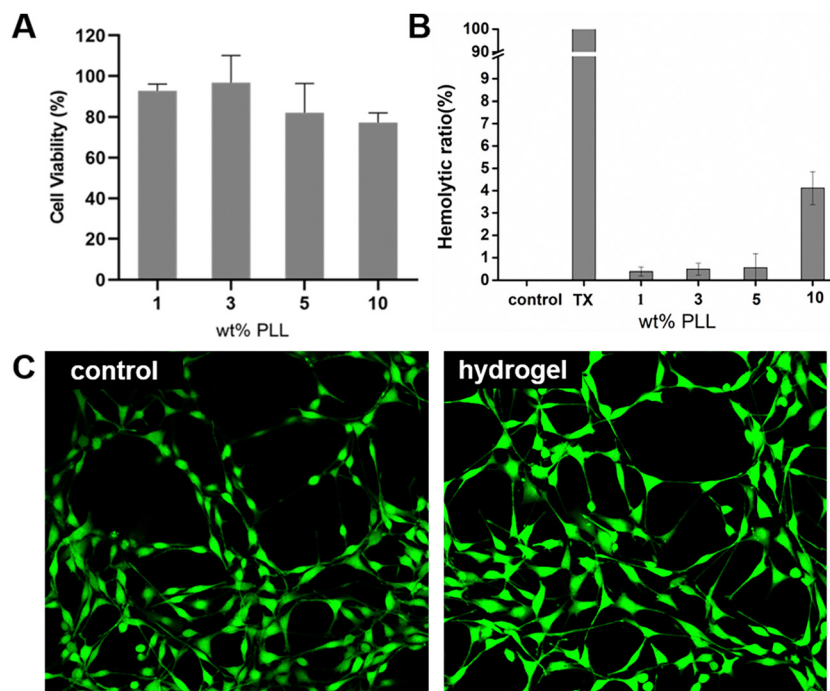


Fig. 4 The biocompatibility of PEG-PLL hydrogels. (A) The cell viability of NIH 3T3 cells after being cultured with PEG-PLL (1), PEG-PLL (3), PEG-PLL (5) and PEG-PLL (10) hydrogel extracts for 24 h. (B) The hemolytic ratio of PEG-PLL (1), PEG-PLL (3), PEG-PLL (5) and PEG-PLL (10) hydrogels. Triton-100 is the positive group. (C) Live/dead cell viability assays to detect the effect of PEG-PLL (5) hydrogels on 3T3 cell viability.

difference in cell morphology between the control and PEG-PLL hydrogel groups.

The biocompatibility of *in situ* forming and antibacterial hydrogels designed for wound dressings is very important. Compared to nano-silver or chitosan hydrogel dressings, we have selected more biocompatible 4-PEG-NHS and PLL materials for constructing hydrogel dressings, of which PLL has been approved by the FDA. The PEG-PLL hydrogel formation process does not require additional crosslinkers. We ultimately chose PEG-PLL (5) hydrogel because it has mechanical properties that match the skin, as well as good antibacterial properties and suitable biocompatibility.

3.5. Antibacterial activity of PEG-PLL hydrogels *in vitro*

The reason that we chose PLL as the antibacterial component is not only its broad-spectrum antibacterial properties, but also because it does not easily result in bacterial resistance. The problem of bacterial resistance has increasingly become a problem that plagues countries around the world. The mechanism of PLL sterilization is to destroy the cell membrane structure of microorganisms through electrostatic action, which causes interruption of the internal material, energy and information transmission of bacterial interactions. It interacts with intracellular ribosomes to affect the synthesis of biological macromolecules, eventually leading to the death of microorganisms and making it less likely to cause bacterial resistance.

To investigate the bactericidal properties of PEG-PLL hydrogels *in vitro*, we performed inhibition zones of the hydrogels.

100 μ L of the bacterial solution (10^7 CFU per mL) was evenly coated on the surface of the TSA, and then PEG-PLL hydrogels with various PLL concentrations were added and incubated at 37 $^{\circ}$ C for 24 h. Then the picture was taken and the size of the inhibition zone was measured. PBS equal to the hydrogel volume was used as the control group. As shown in Fig. 5A and C, all the PEG-PLL hydrogel groups have an antibacterial effect on *S. aureus*, and the size of the inhibition zone of PEG-PLL (1), PEG-PLL (3), PEG-PLL (5) and PEG-PLL (10) is 1.4, 10.1, 12.6, and 13.7 mm respectively. Moreover, there is no significant difference in the size of the inhibition zone between PEG-PLL (5) and PEG-PLL (10). The results indicated that when the concentration of PLL reaches 5% wt, increasing the concentration of PLL cannot enhance the antibacterial ability of the PEG-PLL hydrogel. Similarly, the size of the inhibition zone of PEG-PLL (1), PEG-PLL (3), PEG-PLL (5) and PEG-PLL (10) is 2.1, 5.2, 10.7, and 12.1 mm respectively (Fig. 5B and D). These results indicate that PEG-PLL hydrogels have a good antibacterial effect against both Gram-positive and Gram-negative bacteria *in vitro*.

3.6. Antibacterial activity and wound repair of the PEG-PLL hydrogels *in vivo*

A loss of skin integrity can easily lead to bacteria invading and colonizing a wound. In general, most wound infections are caused by *S. aureus*. Therefore, an SD rat skin full-thickness *S. aureus* infection wound model was used to evaluate the antibacterial and wound repair properties of the PEG-PLL hydrogels. First, a full-thickness skin model with a diameter



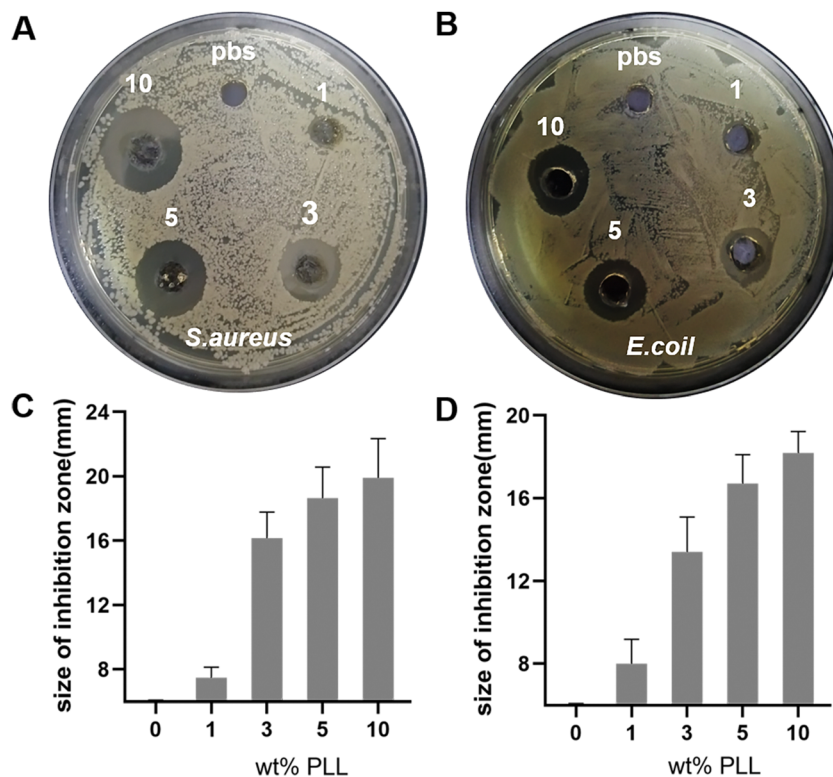


Fig. 5 The PEG–PLL hydrogels with various PLL concentrations against Gram-positive (*S. aureus*) and Gram-negative (*E. coli*) bacteria *in vitro*. (A) The size of the inhibition zone of PEG–PLL hydrogels toward *S. aureus*; (B) the size of the inhibition zone of PEG–PLL hydrogels toward *E. coli*; (C) and (D) statistical significance of the size of the inhibition zone toward *S. aureus* and *E. coli*.

of 10 mm was established. Then the control group used normal saline to simulate the normal tissue repair process. The bacterial group infected with a high concentration of *S. aureus* (10^9 CFU per mL) led to wound infection. The hydrogel group had PEG–PLL (5) applied after two hours of *S. aureus* wound infection. As expected, the hydrogels were very convenient for use in the skin defect, and a transparent gel was formed *in situ*

at the defect in about 10 s. Finally, the wound healing was measured at different time points (4, 7, and 11 d) to investigate its skin healing and antibacterial effects. As shown in Fig. 6A, the PEG–PLL hydrogel group showed accelerated wound closure compared with the control and bacterial group on days 4, 7 and 11. Quantitative analysis of wound closure showed that the percentage of wound closure in the PEG–PLL hydrogel

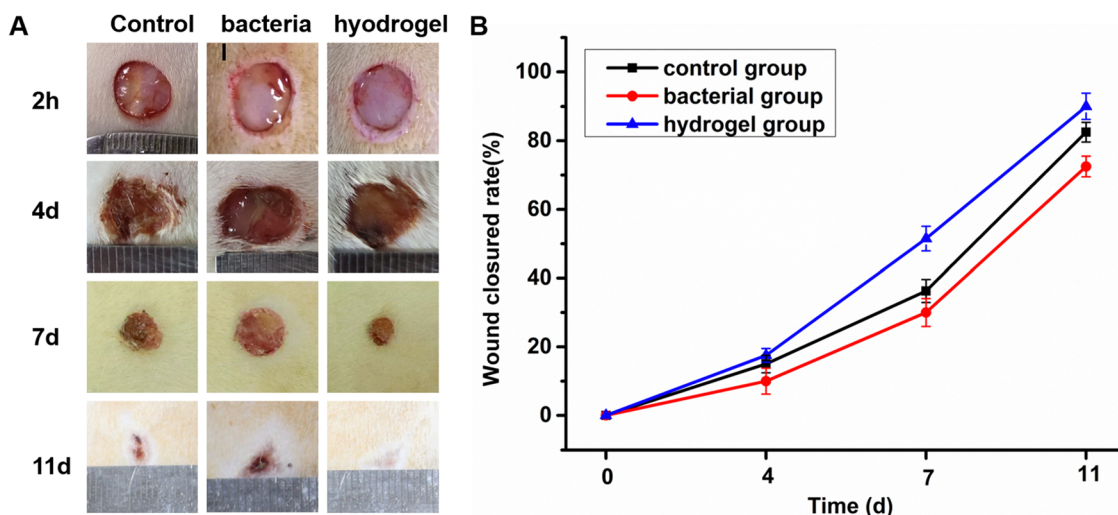


Fig. 6 The wound repair in control, bacterial and PEG–PLL hydrogel groups at different time points (4, 7, and 11 d). (A) Macroscopic observations of wound repair at 4, 7 and 11 days. (B) The wound size closure percent in the three groups at 0, 4, 7 and 11 days.



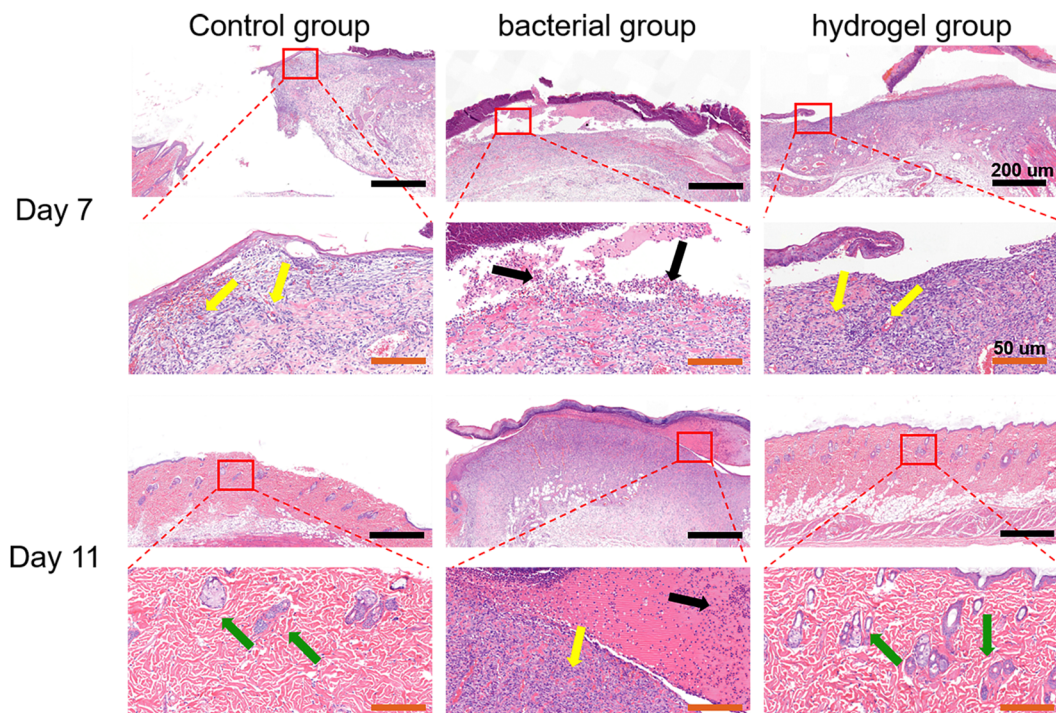


Fig. 7 Histological results of hematoxylin-eosin (H&E) staining in the control, bacterial and hydrogel groups at 7 and 11 days. Black, yellow and green arrows represent *S. aureus* infection, capillaries and skin attachments respectively.

group was significantly higher than the control and bacterial group on days 4, 7 and 11. On day 4, much festering around the wound could be observed in the bacterial group, while the control and hydrogel groups had formed scabs. Moreover, the

hydrogel group healed faster than the control group. On day 11, the wounds in the hydrogel group had healed, while the bacterial group had a slower healing rate with 65% wound closed area. The amount of wound repair in the control,

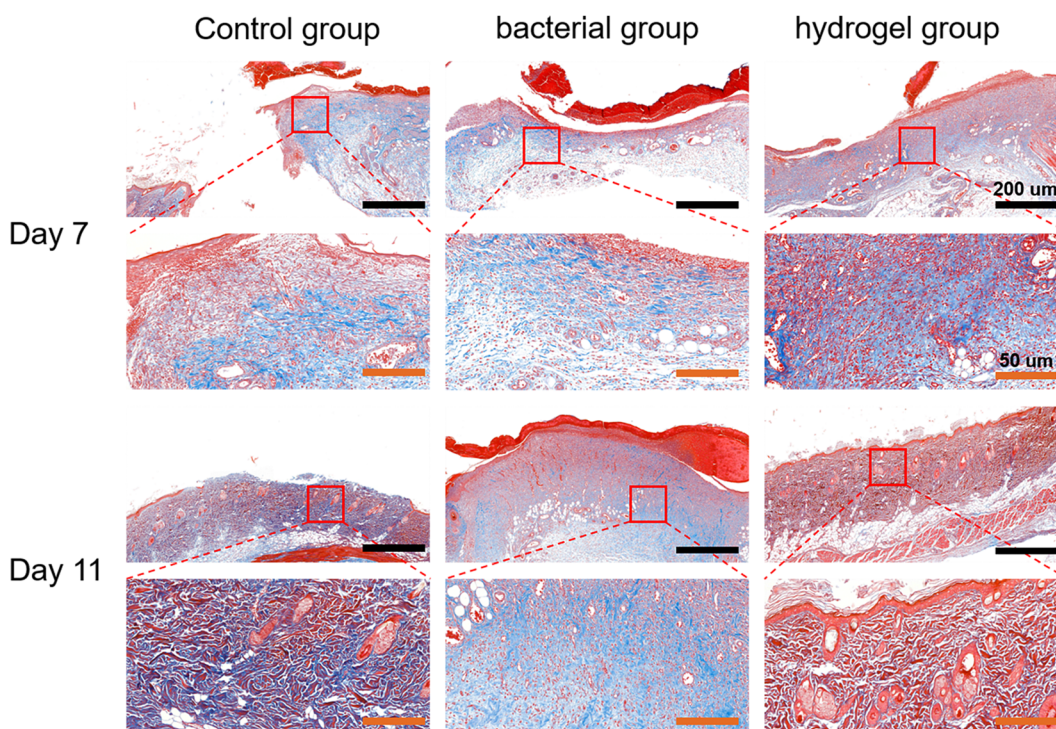


Fig. 8 Histological results of Masson's staining in the control, bacterial and hydrogel groups at 7 and 11 days.



bacterial and PEG-PLL hydrogel groups on day 11 is $82.5 \pm 2.8\%$, $65.5 \pm 2.2\%$, and $91 \pm 2.9\%$ respectively. It has been shown that PEG-PLL hydrogels help promote wound regeneration in *S. aureus*-infected skin.

3.7. The histological results

Histological analysis was first performed using H&E staining. As shown in Fig. 7, there was a large amount of inflammatory cell infiltration and necrotic tissue (black arrows) in the bacterial group indicating severe *S. aureus* infection, while the control and PEG-PLL hydrogel groups showed less inflammatory cell infiltration on day 7. In addition, the control and PEG-PLL hydrogel groups have a larger number of capillaries than the bacterial group (yellow arrows), providing more nutrients for skin regeneration. On day 11, the bacterial groups had a larger number of capillaries, and there was a large amount of inflammatory cell infiltration and necrotic tissue. However, the number of capillaries was significantly reduced in the control and PEG-PLL hydrogel groups. In the early stage of the healing process, a large number of capillaries appeared in the hydrogel group which can provide more nutrients for skin regeneration. After the skin repair is completed, the capillaries will gradually decrease, thereby maintaining the normal metabolism and stability of the skin. Moreover, the control and PEG-PLL hydrogel groups showed the hair follicles, sweat glands, sebaceous glands, and vascular structures of the skin (green arrows), indicating that the skin is completely repaired. There is only a small amount of inflammatory cell infiltration in the subcutaneous tissue of the hydrogel group, which may effectively inhibit the NF- κ B inflammatory pathway and promote tissue repair.

It can be seen from Fig. 8 by Masson staining that the control and PEG-PLL hydrogel groups showed rapid ECM deposition on day 7 (blue collagen). On day 11, collagen fibers in the hydrogel group decreased and were replaced by new regenerated skin attachments, such as hair follicles, sweat glands, sebaceous glands, and vascular structures of the skin, while the bacterial group still had a large number of blue collagen fibers. The reason for this phenomenon is that the *S. aureus* infection will promote the excessive aggregation of inflammatory cells and the activation of TGF- β signaling pathways, causing fibroblasts to differentiate into myofibroblasts and secrete a large amount of type I collagen. The results show that the PEG-PLL hydrogels have good antibacterial activity and wound repair capabilities.

4. Conclusions

In brief, we successfully prepared *in situ* forming hydrogels with antibacterial properties and excellent biocompatibility to accelerate infected wound repair. These *in situ* forming PEG-PLL hydrogels can be easily obtained by mixing 4-arm-poly(ethylene glycol) succinimidyl (4-PEG-NHS) with PLL. The gelling mechanism is through crosslinking of the amine groups of PLL and NHS ester group of 4-PEG-NHS under physiological conditions.

SEM results indicate that the hydrogel has an interconnected porous structure, which facilitates the exchange of nutrients and oxygen with tissues. The swelling results indicate the hydrogels have excellent water absorption and water retention, which can not only absorb a large amount of wound exudate, but also maintain the wound wet environment to accelerate wound repair. The PEG-PLL hydrogel showed a significant antibacterial effect, higher wound closure ratios and collagen deposition in a rat full-thickness skin defect infection model. Furthermore, the cytotoxicity (82.76%) and hemolytic (0.52%) results indicate that PEG-PLL hydrogels have suitable biocompatibility. Notably, the PEG-PLL hydrogels are an ideal wound dressing in clinical work for irregular wound repair, especially for infected wounds.

Conflicts of interest

There are no conflicts to declare.

References

- 1 S. Matorri, A. Veves and D. J. Mooney, *Sci. Transl. Med.*, 2021, **13**, 585.
- 2 A. Zanca, J. M. Osborne, S. G. Zaloumis, C. D. Weller and J. A. Flegg, *Math. Med. Biol.*, 2022, **39**(4), 313–331.
- 3 C. Lindholm and R. Searle, *Int. Wound J.*, 2016, **13**(Suppl 2), 5–15.
- 4 T. Deng, D. Gao, X. Song, Z. Zhou, L. Zhou, M. Tao, Z. Jiang, L. Yang, L. Luo, A. Zhou, L. Hu, H. Qin and M. Wu, *Nat. Commun.*, 2023, **14**(1), 396.
- 5 Y. Qian, Y. Zheng, J. Jin, X. Wu, K. Xu, M. Dai, Q. Niu, H. Zheng, X. He and J. Shen, *Adv. Mater.*, 2022, **34**(29), e2200521.
- 6 Z. Li, J. Lu, T. Ji, Y. Xue, L. Zhao, K. Zhao, B. Jia, B. Wang, J. Wang, S. Zhang and Z. Jiang, *Adv. Mater.*, 2023, e2306350.
- 7 Z. Yang, Y. He, S. Liao, Y. Ma, X. Tao and Y. Wang, *Sci. Adv.*, 2021, **7**, 23.
- 8 W. Cheng, Y. Chen, L. Teng, B. Lu, L. Ren and Y. Wang, *J. Colloid Interface Sci.*, 2018, **513**, 314–323.
- 9 Y. Tu, N. Chen, C. Li, H. Liu, R. Zhu, S. Chen, Q. Xiao, S. Ramakrishna and L. He, *Acta Biomater.*, 2019, **90**, 1–20.
- 10 M. Fursatz, M. Skog, P. Sivler, E. Palm, C. Aronsson, A. Skallberg, G. Greczynski, H. Khalaf, T. Bengtsson and D. Aili, *Biomed. Mater.*, 2018, **13**(2), 25014.
- 11 J. Jin, Z. Ji, M. Xu, C. Liu, X. Ye, W. Zhang, S. Li, D. Wang, W. Zhang, J. Chen, F. Ye and Z. Lv, *ACS Biomater. Sci. Eng.*, 2018, **4**(7), 2541–2551.
- 12 S. Hou, Y. Liu, F. Feng, J. Zhou, X. Feng and Y. Fan, *Adv. Healthcare Mater.*, 2020, **9**(3), e1901041.
- 13 J. Guo, H. Yao, X. Li, L. Chang, Z. Wang, W. Zhu, Y. Su, L. Qin and J. Xu, *Bioact. Mater.*, 2023, **21**, 175–193.
- 14 Z. S. Nishat, T. Hossain, M. N. Islam, H. P. Phan, M. A. Wahab, M. A. Moni, C. Salomon, M. A. Amin, A. A. Sina, M. Hossain, Y. V. Kaneti, Y. Yamauchi and M. K. Masud, *Small*, 2022, **18**(26), e2107571.



- 15 P. Le Thi, Y. Lee, T. T. Hoang Thi, K. M. Park and K. D. Park, *Mater. Sci. Eng. C*, 2018, **92**, 52–60.
- 16 S. Li, S. Dong, W. Xu, S. Tu, L. Yan, C. Zhao, J. Ding and X. Chen, *Adv. Sci.*, 2018, **5**(5), 1700527.
- 17 P. Makvandi, G. W. Ali, S. F. Della, W. I. Abdel-Fattah and A. Borzacchiello, *Carbohydr. Polym.*, 2019, **223**, 115023.
- 18 J. Hoque, B. Bhattacharjee, R. G. Prakash, K. Paramanandham and J. Haldar, *Biomacromolecules*, 2018, **19**(2), 267–278.
- 19 N. Amiri, S. Ghaffari, I. Hassanpour, T. Chae, R. Jalili, R. T. Kilani, F. Ko, A. Ghahary and D. Lange, *Gels*, 2023, **9**, 7.
- 20 S. A. Miner, J. Lee, N. M. Protzman and S. A. Brigido, *Scars Burn Heal*, 2022, **8**, 1467376385.
- 21 Y. Zhou, Y. Miao, Q. Huang, W. Shi, J. Xie, J. Lin, P. Huang, C. Yue, Y. Qin, X. Yu, H. Wang, L. Qin and J. Chen, *Acta Pharm. Sin. B*, 2023, **13**(7), 3153–3167.
- 22 T. Zhu, H. Wang, Z. Jing, D. Fan, Z. Liu, X. Wang and Y. Tian, *Bioact. Mater.*, 2022, **8**, 12–19.
- 23 S. Wang, G. Liu, B. Yang, Z. Zhang, D. Hu, C. Wu, Y. Qin, Q. Dou, Q. Dai and W. Hu, *RSC Adv.*, 2021, **11**(37), 22556–22564.
- 24 Y. Hashimoto, A. Yamashita, J. Negishi, T. Kimura, S. Funamoto and A. Kishida, *ACS Biomater. Sci. Eng.*, 2022, **8**(1), 261–272.
- 25 S. A. Abdulmalek, K. Li, J. Wang, M. K. Ghide and Y. Yan, *Int. J. Mol. Sci.*, 2021, **22**, 21.
- 26 M. Salehizadeh, L. A. Kure, M. Stojmenovic, F. Thei and M. Dong, *Chem. Asian J.*, 2023, **18**(17), e202300515.
- 27 C. Hu, H. Ji, Y. Gong, X. Yang, Y. Jia, Y. Liu, G. Ji, X. Wang and M. Wang, *J. Mater. Chem. B*, 2023, **11**(36), 8666–8678.
- 28 Z. Zou, Z. Zhang, H. Ren, X. Cheng, X. Chen and C. He, *Biomaterials*, 2023, **301**, 122251.
- 29 Y. E. Cheng, I. E. Wu, Y. C. Chen and I. M. Chu, *Gels*, 2022, **8**, 5.
- 30 E. Roeven, A. R. Kuzmyn, L. Scheres, J. Baggerman, M. Smulders and H. Zuillhof, *Langmuir*, 2020, **36**(34), 10187–10199.

